

# Short-Cavity 980 nm DBR Lasers With Quantum Well Intermixed Integrated High-Speed EA Modulators

Chad S. Wang, *Member, IEEE*, Yu-Chia Chang, Uppili Krishnamachari, James W. Raring, *Member, IEEE*,  
and Larry A. Coldren, *Fellow, IEEE*

**Abstract**—Short-cavity, 980 nm distributed Bragg reflector (DBR) lasers with integrated electroabsorption modulators (EAMs) were designed and fabricated using a quantum-well intermixing (QWI) processing platform. Design curves are discussed and the QWI fabrication details are presented. The transmitters exhibited RF bandwidths of 20 GHz and demonstrated error-free operation at 10 Gb/s.

**Index Terms**—Electroabsorption modulators, photonic integrated circuits, quantum well intermixing, semiconductor lasers.

## I. INTRODUCTION

FOR PHOTONICS to replace copper-based electronics in applications such as board-to-board and chip-to-chip level interconnects, there is a clear need for increased speed and efficiency. Traditionally, vertical-cavity surface-emitting lasers (VCSELs) have been the technology of choice for deployment in short-reach data link interconnect applications [1] because of their low power dissipation, ease of coupling, and ability to be integrated into arrays. However, in these traditional interconnect systems, most of the power consumption occurs over the receiver electronics, namely over transimpedance amplifiers. An alternative method to reduce the overall power consumption of the link is to use a “receiver”-less architecture to eliminate the receiver electronics. This requires high-output power transmitters to directly drive detectors controlling the decision circuits.

In order to achieve a high-power, high-speed, and low-power dissipation single-mode transmitter, we propose a short-cavity distributed Bragg reflector (DBR) laser structure with an integrated electroabsorption modular (EAM) to meet these requirements. This design crosses the advantages of VCSELs and edge-emitters. By reducing the active volume of the laser cavity, the efficiency of the device is improved, to a point where the mirror reflectivity must be increased. VCSELs have demonstrated high efficiencies, but operation to higher data rates is challenging. For VCSELs, the highest data rate reported is 25 Gb/s [2]. Edge-emitters with integrated EAMs have shown operation at 40

Manuscript received November 1, 2006; revised July 22, 2007. This work was supported in part by the Defense Advanced Research Projects Agency under Chip-to-Chip Optical Interconnects.

C. S. Wang, Y.-C. Chang, U. Krishnamachari, and L. A. Coldren are with the Electrical and Computer Engineering Department, University of California, Santa Barbara, CA 93106 USA (e-mail: cswang@engineering.ucsb.edu).

J. W. Raring was with the Materials Department, University of California, Santa Barbara, CA 93106 USA. He is now with Sandia National Laboratories, Albuquerque, NM 87123 USA.

Digital Object Identifier 10.1109/JSTQE.2007.905095

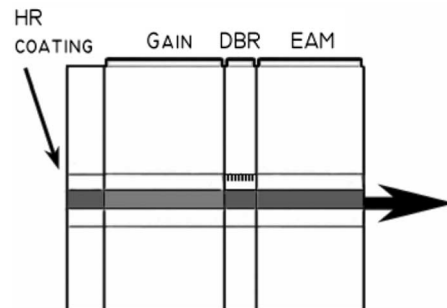


Fig. 1. Schematic cross section of DBR laser device with integrated EAM. Indicated are the sections of the DBR laser-EAM transmitter.

Gb/s. We have previously demonstrated high efficiency, short-cavity DBR lasers at 1.55  $\mu\text{m}$  with integrated, high-bandwidth (25 GHz) EAMs [3]. By using a quantum-well intermixing (QWI) integration platform, the laser and modulator can be simultaneously optimized for high performance. Recently, 980 nm DBR lasers with quantum well intermixed passive sections have been demonstrated with output powers up to 400 mW [4]. Moreover, intermixed quantum well (QW) EAMs have also shown promise to extend data rates up to 40 Gb/s and beyond [5]. Here, we present a short-cavity, 980 nm, DBR laser using a QWI platform in the InGaAs/GaAs/AlGaAs material system, monolithically integrated with a high-speed EAM demonstrating 20 GHz of 3 dB bandwidth. Design curves are discussed and the QWI fabrication details are presented.

## II. EXPERIMENT

### A. Short-Cavity DBR Laser Design

We propose a short-cavity DBR laser with integrated EAM designed with three sections: gain, front DBR mirror, and EAM, with a high reflectivity (HR) coating applied to the rear facet of the DBR, as shown in the side-view schematic of Fig. 1. In designing a short-cavity laser, tradeoffs exist between the operating current as a function of mirror reflectivity and active region length. We can begin by simulating the operating current  $I$  as a function of front mirror reflectivity  $R_1$  or equivalently, mirror length, as described by

$$I = \frac{qP_o(\alpha_i + \alpha_m)}{F_1\eta_i h \nu \alpha_m} + I_{th} \quad (1)$$

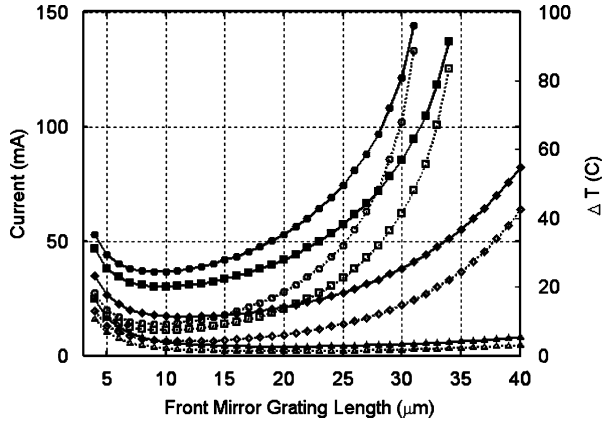


Fig. 2. Design curve of operating current (solid lines) and on-chip temperature rise (dotted lines) vs. front mirror grating length for a family of output powers at 1 mW (triangles), 10 mW (diamonds), 20 mW (squares), and 25 mW (circles). The active region length was set at  $110 \mu\text{m}$  and  $\kappa$  of  $650 \text{ cm}^{-1}$ .

where  $P_o$  is the output power,  $\alpha_i$  is the internal loss,  $\alpha_m$  is the mirror loss,  $F_1$  is the fractional power out the front mirror,  $\eta_i$  is the injection efficiency, and  $I_{\text{th}}$  is the threshold current [6].  $I_{\text{th}}$  can be solved using the gain equation,

$$I_{\text{th}} = wL_a N J_{\text{tr}} \exp \left( \frac{(\alpha_i + \alpha_m)L}{\Gamma g_o L_a} \right) \quad (2)$$

where  $w$  is the ridge width,  $L_a$  is the active region length,  $L$  is the total cavity length,  $N$  is the number of quantum wells,  $J_{\text{tr}}$  is the transparency current density,  $\Gamma$  is the confinement factor, and  $g_o$  is the material gain. Values of  $15 \text{ cm}^{-1}$ , 90%, 70 A/cm<sup>2</sup>,  $50 \text{ cm}^{-1}$ , and 80% were used for  $\alpha_i$ ,  $\eta_i$ ,  $J_{\text{tr}}$ ,  $\Gamma g_o$ , and the rear HR mirror,  $R_2$ , respectively. As shown in Fig. 2,  $I$  can be plotted as a function of front mirror grating length for a fixed active region length. The on-chip temperature rise,  $\Delta T$ , can also be simulated as given in (3) and iterated with (4) to find the equilibrium operating current [6].

$$\Delta T = (IV_d + I^2 R_s - P_o) Z_t \quad (3)$$

$$I = I_{\text{th}} + I_{\text{po}} \exp \left( \frac{T}{T_1} \right). \quad (4)$$

Assuming the light output power increases linearly with injection current above threshold, (4) is a modified form of the traditional temperature dependence equation for differential quantum efficiency,  $\eta_d(T) = \eta_{do} \exp(s - T/T_1)$ , obtained by substituting the equation for output power,  $P_o = \eta_d (h\nu/q)(I - I_{\text{th}})$ .  $I_{\text{th}}$  can be represented by the threshold temperature dependence,  $I_{\text{th}}(T) = I_0 \exp(T/T_0)$ .  $T_0$  is the characteristic temperature,  $T_1$  is the characteristic temperature for the above-threshold current increment,  $I_0$  and  $I_{\text{po}}$  are constants, and  $Z_t$  is the thermal impedance, which we have assumed to be  $3.46/L_a \cdot \text{°C/W}$ , using a thermal conductivity of  $0.45 \text{ W/cm} \cdot \text{°C}$  [6]. We have assumed  $T_0$  and  $T_1$  to be 100 K and 200 K, respectively. As can be seen from Fig. 2, there lies an ideal front mirror length that gives the lowest operating current for a given active region length. Solving for the ideal front mirror length of each active region length, we can then solve (1) as a function

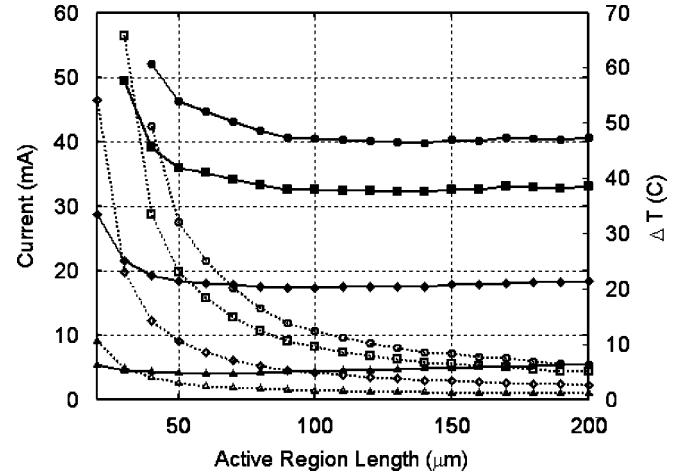


Fig. 3. Design curve of operating current (solid lines) and on-chip temperature rise (dotted lines) vs. active region length for a family of output powers at 1 mW (triangles), 10 mW (diamonds), 20 mW (squares), and 25 mW (circles). The front mirror length was optimized for each active region length at a  $\kappa$  of  $650 \text{ cm}^{-1}$ .

of active region length, as shown in Fig. 3. This shows that the active region length for a short-cavity DBR laser can be reduced to as low as  $50 \mu\text{m}$  before the operating current and on-chip temperature rise begins to increase sharply.

From these simulations we have designed the gain section of the device at  $110 \mu\text{m}$ . A front DBR of  $20 \mu\text{m}$  length was chosen, making use of deep gratings aimed at  $40 \text{ nm}$  etch depth, and targeting a coupling coefficient  $\kappa$  of  $650 \text{ cm}^{-1}$ . This DBR length is chosen to be slightly larger than the optimum minimum shown in Fig. 2 in order to compensate for fabrication and regrowth error [7]. Lastly, the transmitters were fabricated with  $125 \mu\text{m}$  long EAMs. Passive waveguides were also included to facilitate postprocess cleaving and coating.

## B. Quantum Well Intermixing Background

There are several main techniques used to accomplish QWI: ion-implantation enhanced interdiffusion (IIEI), impurity-induced disordering (IID), and impurity-free vacancy-enhanced disordering (IFVD). All are based on the generation of vacancies and its diffusion through the QW active region by a rapid thermal anneal (RTA). The IIEI method relies on the diffusion of point defects created during an ion implantation. This method can utilize implant energies ranging from tens of kiloelectronvolts up to megaelectronvolts, and has been shown to have good spatial resolution. The range of intermixing is also very controllable using anneal time, temperature, and implant dose [8], [9]. This process has been used with great success in developing high functionality wavelength-agile PICs on InP [3]. Moreover, impurity-free IIEI processes have also been translated to GaAs with some success [10], [11].

The IID method uses impurities, commonly dopants, to change the equilibrium defect concentration, which is dependent on the Fermi level, to enhance the group III or group V self-diffusion in the crystal, thereby promoting the intermixing [12]. Recently, IID has been applied to 980 nm VCSELs with modest

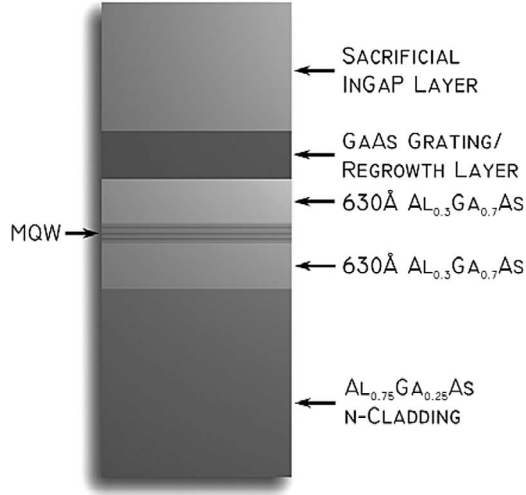


Fig. 4. Epitaxial base structure with three-QW active region.

success; however, the introduction of dopants used to promote intermixing could have adverse effects on the electrical nature of the devices structure [13], [14].

In this paper, we employ an impurity-free vacancy-enhanced disordering method, using a  $\text{SiO}_2$  dielectric cap. Previous literature has shown intermixing to occur with a variety of deposition techniques, such as plasma-enhanced chemical vapor deposition (PECVD) or sputter deposition [12], [15]. All approaches use the concept of Ga outdiffusion into the  $\text{SiO}_2$  capping layer, which creates vacancies in the group III sublattice which can then diffuse down to the QW region. Similar to the other intermixing techniques, IFVD can be performed on full laser structures, where the vacancies must diffuse long distances through the entire upper p-cladding before reaching the quantum wells. Although this is not detrimental to the intermixing itself, the device performance may be hindered by the redistribution of precisely placed doping interfaces. We have taken an approach which uses a partially grown laser structure and a sacrificial cap layer, which can be subsequently removed and the upper cladding regrown [9]. This approach is also advantageous for integrating gratings within the laser to precisely control the coupling and reflectivity. Recent work has demonstrated high power DBR lasers with intermixed passive sections [4].

We will show that by using a selective IFVD QWI processing platform, a DBR laser with EAM can be monolithically integrated into a single transmitter device.

### III. PROCESS

The epitaxial base structure, as shown in Fig. 4, was grown on a silicon doped GaAs substrate by molecular beam epitaxy (MBE). The active region consists of three 8 nm thick  $\text{In}_{0.18}\text{Ga}_{0.82}\text{As}$  quantum wells with 8 nm GaAs barriers centered between  $\text{Al}_{0.3}\text{Ga}_{0.7}\text{As}$  waveguide layers. The upper waveguide also includes a 65 nm GaAs layer used as a gratings and aluminum-free regrowth layer, followed by a 300 nm undoped sacrificial InGaP layer.

The intermixing process began by first subjecting the sample to a blanket surface fluorination treatment. This was done in a reactive ion etching plasma with  $\text{SF}_6$  gas to create In-F and Ga-F bonds on the sample surface without etching the semiconductor [16], [17]. Next,  $\text{SiO}_2$  was deposited by PECVD and used as a hard mask. In the passive regions, or areas of the sample to be intermixed, the  $\text{SiO}_2$  was etched off using BHF and a developer (basic) solution was used to remove the fluorine bonds. Lastly, another layer of  $\text{SiO}_2$  was deposited by PECVD. Intermixing then occurred during the RTA, whereby areas of the sample that were in direct contact with the  $\text{SiO}_2$  yielded a blue-shift in the photoluminescence spectra. The areas of the sample that still possessed the fluorine bonds remained at the as-grown band-edge because it prevented group-III outdiffusion into the  $\text{SiO}_2$ . The reason for covering the entire sample with  $\text{SiO}_2$  was to prevent arsenic decomposition from the sample during the high-temperature RTA. Additional details of the intermixing process can be found in [18].

Following QWI of the passive waveguide, DBR, and EAM sections, the sacrificial InGaP layer is removed by wet selective etching, and first order gratings are patterned using an immersion holography technique and dry etched into the GaAs regrowth layer [7]. A 2  $\mu\text{m}$  regrowth of the upper p-cladding and p-contact was performed by MBE [7]. Ridge waveguides 3  $\mu\text{m}$  wide were patterned, benzocyclobutene (BCB) was defined beneath the EAM contacts for low capacitance, and isolation was accomplished by proton implantation. The wafers were thinned, backside metalized, and cleaved into bars. Subsequently, the front and rear facets of cleaved bars were AR and HR-coated, respectively. Finally, the devices were mounted onto AlN carriers and wire-bonded to RF pads for high-speed testing. Including passive waveguides, the entire transmitter totaled around 425  $\mu\text{m}$  in length.

## IV. EXPERIMENTAL RESULTS

### A. QWI

The intermixing process was calibrated using several samples cleaved from the base structure, as described in the previous section. These samples were annealed at 800 and 850  $^\circ\text{C}$  for various times ranging from 10 to 180 s and the extent of the intermixing was measured by room-temperature photoluminescence. As can be seen in Fig. 5, the intermixing occurs rapidly within the first 30 s, then begins to saturate with increasing time. With greater anneal temperatures, intermixing occurs at a faster rate; greater overall amount of intermixing is obtainable due to an increased diffusion coefficient and Ga outdiffusion in the  $\text{SiO}_2$ . Assuming intermixing occurs only on the group III sublattice for InGaAs/GaAs QWs, we calculate the maximum obtainable amount of intermixing to be 40 nm [19].

The DBR lasers with integrated EAMs fabricated using this selective intermixing process had an active band-edge at  $\lambda_{\text{pl}} = 977$  nm and a passive band-edge at  $\lambda_{\text{pl}} = 949$  nm. The EAMs used the same band-edge as the passive section. While this process can be used to selectively achieve two band-edges on chip, repeating the process to achieve multiple or intermediate band-edges have not been successful as in [11].

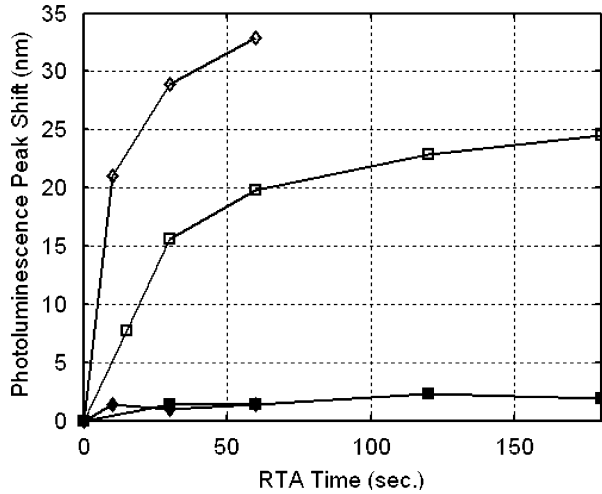


Fig. 5. Photoluminescence peak shift as a function of anneal temperature and time. Open and closed symbols indicate intermixed and nonintermixed at anneal temperatures of 800 °C (squares) and 850 °C (diamonds).

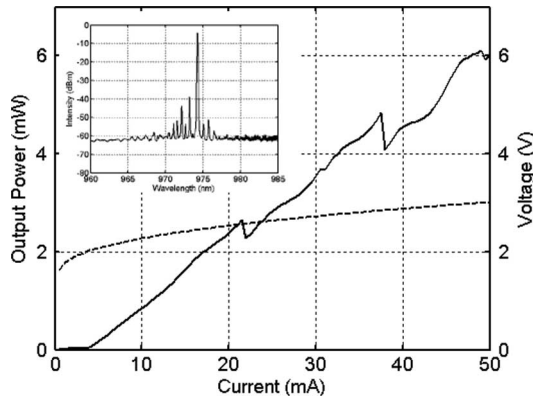


Fig. 6. Room temperature CW light (solid) and voltage (dashed) characteristics of the integrated DBR laser-modulator. The inset shows the single mode lasing spectrum at 35 mA bias.

### B. DBR Laser

Operating in continuous wave (CW) mode, the DBR laser exhibited single mode lasing at 975 nm with greater than 30 dB side-mode suppression ratio, as targeted from the design. The mode spacing of  $\sim 6$  Å is slightly lower than the estimated mode spacing of  $\sim 7$  Å, indicating weaker reflection from the DBR section resulting in a longer cavity length. The additional spurious modes are due to reflections from the front facet.

The lasers also exhibited a threshold current of 5 mA and demonstrated output powers up to 6 mW at a gain section current of 50 mA, as shown in Fig. 6. We believe the low output powers of these devices are due to nonoptimal regrowth conditions, where both interface cleanliness and gratings overgrowth can be improved. Furthermore, we expect to see higher output powers upon improving the low injection efficiency of these devices, currently down at around 50%, which were measured from test ridge laser structures fabricated on the same chip. The higher voltage turn-on was due to high contact resistance resulting from damage to the contact layer during processing.

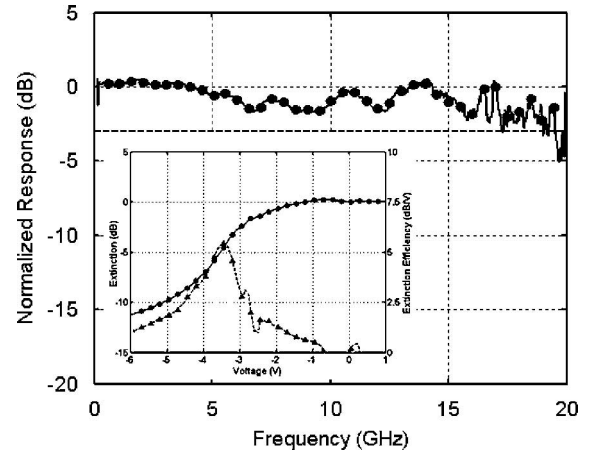


Fig. 7. Bandwidth curve showing 20 GHz of  $-3$  dB bandwidth for a 125  $\mu\text{m}$  long EAM. The inset shows the corresponding DC extinction curve.

The kinks in the output power were due to mode hopping. This was observed in the lasing spectrum, and can be explained from red shifting of the reflection spectrum with on-chip temperature rise. Using (3), the kinks occurring at 22 and 38 mA correspond to a 17 and 33 °C on-chip temperature rise, respectively. Assuming the refractive index changes with temperature by  $1.2e-4/^\circ\text{C}$  for AlGaAs, then the change in center wavelength of the grating with change in the index is 6.1 and 11.8 Å, respectively, equal to the mode spacing of the laser. With future improvement on the material quality, as well as reducing the excess voltage drop, less power would be dissipated in the device, leading to lower on-chip temperature rise and fewer kinks in the output power.

### C. EA Modulator

As can be seen in the inset in Fig. 7, the 125  $\mu\text{m}$  long integrated EAMs exhibited over 10 dB of optical extinction at  $-5$  V with a peak extinction efficiency of 5 dB/V at  $-3.5$  V. Fig. 7 also shows the small signal 3dB modulation bandwidth measured to be 20 GHz. Large signal digital modulation experiments were performed at 10 Gb/s using a nonreturn to zero pattern and a pseudorandom-bit-sequence of  $2^{31}-1$ . Open eye diagrams were achieved with 7.7 dB dynamic extinction at a DC bias of  $-2.5$  V and a 3 V peak-to-peak swing. Corresponding bit error rate (BER) curve is plotted in Fig. 8, demonstrating error-free operation down to  $10^{-10}$ . Higher data rates were not able to be tested due to equipment limitations; however, we expect data rates up to 30 Gb/s possible with the demonstrated bandwidths. Extinction ratios and extinction efficiency can also be improved with less intermixing of the EAM band-edge, resulting in bringing the exciton peak and absorption edge closer to the lasing wavelength [20], [21].

## V. CONCLUSION

We have demonstrated short-cavity DBR lasers emitting at 980 nm with integrated QW-EA modulators fabricated using a QWI platform. Short-cavity DBR lasers present a solution for achieving higher power lasers for use in “receiver”-less data link

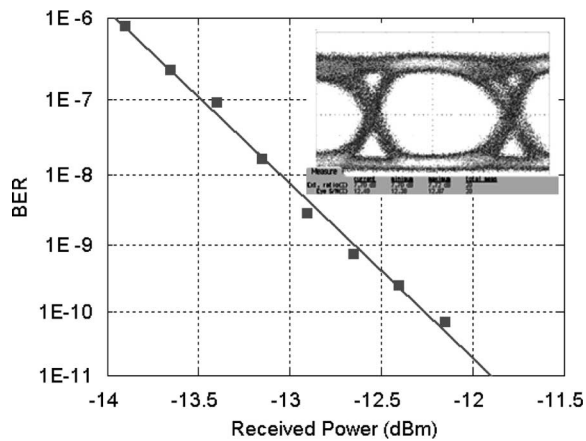


Fig. 8. BER curve showing 10 Gb/s error-free operation down to  $1e-10$ . The inset shows corresponding eye at 10 Gb/s.

interconnect architectures. A QWI processing platform is used for integration and is capable of achieving greater than 30 nm of shift between the active and passive band-edges on a chip. The integrated QWI EAMs demonstrated 20 GHz bandwidth and error-free operation at 10 Gb/s, with further optimization possible for increased high-speed performance. With QWI, the band-edge of each section of the device can be individually optimized, resulting in monolithic integration of lasers with high-performance QW-EAMs.

## REFERENCES

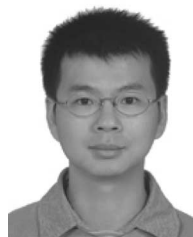
- [1] J. Kash *et al.*, "Chip-to-chip optical interconnects," presented at the Opt. Fiber Commun. Conf., Tech. Dig., 2006, Paper OFA3.
- [2] N. Suzuki, H. Hatakeyama, K. Fukatsu, T. Anan, K. Yashiki, and M. Tsuji, "25-Gbps operation of 1.1- $\mu$ m-range InGaAs VCSELs for high-speed optical interconnections," presented at the Opt. Fiber Commun. Conf., Tech. Dig., 2006, Paper OFA4.
- [3] E. J. Skogen, J. W. Raring, G. B. Morrison, C. S. Wang, V. Lal, M. Mašanović, and L. A. Coldren, "Monolithically integrated active components: A quantum well intermixing approach," *IEEE J. Sel. Topics Quantum Electron.*, vol. 11, no. 2, pp. 343–355, Mar./Apr. 2005.
- [4] K. Song, Y. Li, N. Visovsky, M. Hu, H. K. Nguyen, X. Liu, S. Coleman, B. Paddock, M. Turner, C. Catherine, R. Bhat, and C. E. Zah, "High power 1060 nm DBR lasers with quantum well intermixed passive sections," in *Proc. 18th Annu. Meeting IEEE Lasers Electro-Opt. Soc.*, Oct. 23–27, 2005, pp. 949–950.
- [5] J. W. Raring, L. A. Johansson, E. J. Skogen, M. N. Sysak, H. N. Poulsen, S. P. DenBaars, and L. A. Coldren, "Low drive voltage, negative chirp 40 Gb/s EA-modulator/widely tunable laser transmitter, using quantum-well intermixing," presented at the Opt. Fiber Commun. Conf. Tech. Dig., 2006, Postdeadline Paper PDP26.
- [6] L. A. Coldren and S. W. Corzine, *Diode Lasers and Photonic Integrated Circuits*. New York: Wiley, 1995.
- [7] C. S. Wang, G. B. Morrison, E. J. Skogen, and L. A. Coldren, "Fabrication and molecular beam epitaxy regrowth of first-order high contrast AlGaAs/GaAs gratings," *J. Vac. Sci. Technol.: B*, vol. 24, no. 3, pp. 1559–1563, 2006.
- [8] S. Charbonneau, P. J. Poole, P. G. Piva, G. C. Aers, E. S. Koteles, M. Fallahi, J. He, J. P. McCaffrey, M. Buchanan, and M. Dion, "Quantum-well intermixing for optoelectronic integration using high energy ion implantation," *J. Appl. Phys.*, vol. 78, no. 6, p. 3697, 1995.
- [9] E. J. Skogen, J. S. Barton, S. P. DenBaars, and L. A. Coldren, "A quantum-well-intermixing process for wavelength-agile photonic integrated circuits," *IEEE J. Sel. Topics Quantum Electron.*, vol. 8, no. 4, pp. 863–869, Jul./Aug. 2002.
- [10] P. G. Piva, R. D. Goldberg, I. V. Mitchell, S. Fafard, M. Dion, M. Buchanan, S. Charbonneau, G. Hillier, and C. Miner, "Reduced 980 nm laser facet absorption by band gap shifted extended cavities," *J. Vac. Sci. Technol. B*, vol. 16, no. 4, pp. 1790–1793, Jul. 1998.
- [11] E. J. Skogen, L. A. Coldren, J. W. Raring, and S. P. DenBaars, "Multiple-band-edge quantum-well intermixing in the InGaAs/InGaAsP/InGaP material system," *Appl. Phys. Lett.*, vol. 86, pp. 241117-1–241117-3, 2005.
- [12] D. Deppe and N. Holonyak, Jr., "Atom diffusion and impurity-induced layer disordering in quantum well III–V semiconductor heterostructures," *J. Appl. Phys.*, vol. 64, pp. 93–113, 1988.
- [13] R. L. Naone, P. D. Floyd, D. B. Young, E. R. Hegblom, T. A. Strand, and L. A. Coldren, "Interdiffused quantum wells for lateral carrier confinement in VCSEL's," *IEEE J. Sel. Topics Quantum Electron.*, vol. 4, no. 4, pp. 706–714, Jul./Aug. 1998.
- [14] D. D. Lofgreen, Y.-C. Chang, and L. A. Coldren, "Vertical-cavity surface-emitting lasers with lateral carrier confinement," *Inst. Electr. Eng. Electron. Lett.*, vol. 43, no. 3, pp. 163–164, Feb. 2007.
- [15] S. D. McDougall, O. P. Kowalski, C. J. Hamilton, F. Camacho, B. Qiu, M. Ke, R. M. De La Rue, A. C. Bryce, and J. H. Marsh, "Monolithic integration via a universal damage enhanced quantum-well intermixing technique," *IEEE J. Sel. Topics Quantum Electron.*, vol. 4, no. 4, pp. 636–646, Jul./Aug. 1998.
- [16] D. D. Lofgreen, "Investigation of selective quantum well intermixing in vertical cavity lasers," Ph.D. dissertation, Univ. California, Santa Barbara, 2004.
- [17] L. R. Williston, I. Bello, and W. M. Lau, "X-ray photoelectron spectroscopic study of the interactions of  $CF^+$  ions with gallium arsenide," *J. Vac. Sci. Technol. A*, vol. 11, no. 4, pp. 1242–1247, 1993.
- [18] C. S. Wang, Y.-C. Chang, J. W. Raring, and L. A. Coldren, "Short-cavity 980 nm DBR lasers with quantum well intermixed integrated high-speed EA modulators," in *Proc. Int. Semicond. Laser Conf.*, 2006, pp. 129–130.
- [19] J. W. Raring, "Advanced InP based monolithic integration using quantum well intermixing and MOCVD regrowth," Ph.D. dissertation, Univ. California, Santa Barbara, 2006.
- [20] G. B. Morrison, C. S. Wang, E. J. Skogen, D. D. Lofgreen, and L. A. Coldren, "980 nm DBR lasers monolithically integrated with EA modulators for optical interconnect applications," presented at the Integr. Photon. Res. Appl., 2005, Paper IWF2.
- [21] G. B. Morrison, E. J. Skogen, C. S. Wang, J. W. Raring, Y.-C. Chang, M. Sysak, and L. A. Coldren, "Photocurrent spectroscopy for quantum-well intermixed photonic integrated circuit design," *IEEE Photon. Technol. Lett.*, vol. 17, no. 7, pp. 1414–1416, Jul. 2005.



photodetectors.

**Chad S. Wang** (S'99–M'07) received the B.S. degree from the University of Texas at Austin, in 2001 and the M.S. degree from the University of California, Santa Barbara, in 2002, where he is currently working toward the Ph.D. degree in electrical and computer engineering.

His current research interests focus on the development of integrated laser modulators for optical interconnect applications. He is also involved in molecular beam epitaxial growth of III–V semiconductors, including vertical-cavity lasers and avalanche



optical interconnect applications.

**Yu-Chia Chang** received the B.S. in electrical engineering and M.S. degree in electro-optical engineering from National Taiwan University in 1997 and 1999, respectively. He worked for BenQ Inc., Taiwan during 1999–2001 and National Taiwan University during 2001–2002. He is currently working toward the Ph.D. degree in electrical and computer engineering at the University of California, Santa Barbara.

His current research interests are the design, growth, and characterization of high-efficiency, high-speed vertical-cavity surface-emitting lasers for optical interconnect applications.

**Uppili Krishnamachari**, photograph and biography not available at the time of publication.



**James W. Raring** (M'00) received his B.S. degree in materials engineering from California Polytechnic State University, San Luis Obispo, in 2001 and the Ph.D. in materials science from the University of California, Santa Barbara, in 2006. His dissertation focused on the design, growth, and fabrication of high-functionality wavelength-agile InGaAsP based photonic integrated circuits (PIC).

By coupling quantum well intermixing with MOCVD regrowth, he combined widely tunable sampled grating DBR lasers, 40 Gb/s electroabsorption modulators, low-confinement high-saturation power semiconductor optical amplifiers, and 40 Gb/s untraveling carrier photodiodes to demonstrate the first single-chip 40 Gb/s optical transceiver. In 2006, James joined the RF/optoelectronic group at Santa National Laboratories where he continues to work on leading edge PICs. He has authored or co-authored over 75 technical papers and is a member of IEEE LEOS, OSA and SPIE.



**Larry A. Coldren** (M'00) received the Ph.D. degree in electrical engineering from Stanford University in 1972.

After 13 years of research at Bell Laboratories, he joined UCSB in 1984 where he now holds appointments in Materials and Electrical & Computer Engineering, and is Director of the Optoelectronics Technology Center. He is the Fred Kavli Professor of Optoelectronics and Sensors at UCSB. In 1990 he cofounded Optical Concepts, later acquired as Gore Photonics, to develop novel VCSEL technology; and in 1998 he cofounded Agility Communications, recently acquired by JDSU, to develop widely tunable integrated transmitters. At Bell Labs, he initially worked on waveguided surface-acoustic-wave signal processing devices and couple-resonator filters. He later developed tunable coupled-cavity lasers using novel reactive-ion etching (RIE) technology that he created for the then new InP-based materials. At UCSB he continued work on multiple-section tunable lasers, in 1988, inventing the widely tunable multielement mirror concept. During the late eighties he also developed efficient vertical-cavity multiple-quantum-well modulators which led to novel vertical-cavity surface-emitting laser (VCSEL) designs that provided unparalleled levels of performance. He continues to be active in developing new photonic integrated circuit (PIC) and VCSEL technology, including the underlying materials growth and fabrication techniques. In recent years, for example, he has been involved in the creation of efficient all-epitaxial InP-based and high-modulation speed GaAs-based VCSELs as well as a variety of InP-based PICs incorporating numerous optical elements for widely tunable integrated transmitters, receivers, and wavelength converters operating up to 40 Gb/s. He has authored or coauthored over 800 papers, five book chapters, one textbook, and has been issued 61 patents. He has presented dozens of invited and plenary talks at major conferences.

Prof. Coldren is a member of Optical Society of America and the recipient of the Institution of Electrical Engineers, 2004 John Tyndall Award, and a member of the National Academy of Engineering.